Annales Societatis Geologorum Poloniae (2025), vol. 95: 17–28 https://doi.org/10.14241/asgp.2025.02

INTEGRATED GEOPHYSICAL RESEARCH IN A PROFILE CROSSING THE MÉLANGE BELT WITHIN THE PIENINY KLIPPEN BELT – A CASE STUDY

Monika ŁÓJ*, Sławomir PORZUCEK, Grzegorz BANIA & Kamil CICHOSTĘPSKI

AGH University of Krakow, Faculty of Geology,
Geophysics and Environmental Protection,
Mickiewicza 30, 30 –059 Kraków, Poland;
e-mails: mloj@agh.edu.pl, porzucek@agh.edu.pl,
bania@agh.edu.pl, kcichy@agh.edu.pl
** Corresponding author*

Łój, M., Porzucek, S., Bania, G. & Cichostępski, K., 2025. Integrated geophysical research in a profile crossing the mélange belt within the Pieniny Klippen Belt – a case study. *Annales Societatis Geologorum Poloniae,* 95: 17–28.

Abstract: The primary objective of the research was to identify geological structures within the mélange belt and determine whether the carbonate rock outcrops visible at the surface are olistoliths. The study was carried out along a 1-km profile that crossed the mélange zone perpendicularly. Three geophysical methods (gravity, geoelectric and seismic) were applied to solve the problem. Each of these methods follows different physical properties of rocks; therefore, the results should complement each other, although they may not always be fully compatible. The results obtained from all methods allowed the identification of zones with varying physical properties, which can be associated with known geological formations. As described above, each method also detected changes in physical properties within the mélange zone, caused by lime rock outcrops. An integrated analysis of the results of all three methods revealed a very high correlation in the boundaries of the identified zones, significantly validating the final geological interpretation. The findings also confirmed that the rock outcrops observed at the surface are in fact olistoliths embedded in a matrix, much like "raisins in a cake".

Key words: Gravimetry, seismic refraction tomography (SRT), electrical resistivity tomography (ERT), olistolith.

Manuscript received 12 November 2025, accepted 17 March 2025

INTRODUCTION

The research area is located in southern Poland, south of Kraków, east of Nowy Targ, near Krempachy, in the boundary area between two major structural units. The geophysical methods that were used in this research were gravity, geoelectric, and seismic surveys. Previous geological and geophysical studies of this area revealed the existence of two major structural units, the Central and Outer Carpathians, separated by the Pieniny Klippen Belt (Golonka *et al.*, 2018, 2019).

This region has been explored many times, using geophysical methods, such as the seismic method, gravity method, geoelectric method, and magnetic method. The gravity method, tracking the density changes, was used especially to investigate the geological background (Grabowska *et al.*, 2007; Stefaniuk *et al.*, 2007; Mikołajczak *et al.*, 2021) and lineaments or structural boundaries (Porzucek *et al.*, 2023).

In 2015, a deep reflection seismic survey "Czorsztyn 2D" was conducted in the study area. These were the first high-resolution studies, carried out in the Pieniny Klippen Belt region (Golonka *et al.*, 2019; Marzec *et al.*, 2020). The main aim of the studies was to research the structure of three main Carpathian tectonic units (Central Carpathians, Pieniny Klippen Belt and Outer Carpathians) in the suture zone. The results obtained, apart from deep structural interpretation (Golonka *et al.*, 2019), allowed determination of the position of the olistoliths, based on seismic data.

Of particular interest for the present study is the Pieniny Klippen Belt (PKB), which has a complex geological structure. The PKB zone is a mixture of rock elements of various origins, defined as mélange. The study of this mélange is essential for the description of the regional geology, palaeogeography, and evolution, as the description of the nature of the PKB is still controversial (Golonka *et al.*, 2022 and references therein). A knowledge of mélange structures reveals their role in the geodynamics of the PKB belt and the tectonic and sedimentary processes that created this belt. The

latest geophysical research to identify the mélange was described in Bania and Mościcki (2024), Bania *et al.* (2024), Łój *et al.* (2024), and Cichostępski *et al.* (2024a, b). This article presents an integrated geophysical interpretation of the geological structures, using gravity, geoelectric, and seismic methods for a single selected survey line.

GEOLOGICAL SETTINGS

The Pieniny Klippen Belt (PKB) is a very narrow and long boundary zone between the Central and Outer Carpathians (Golonka and Krobicki, 2004; Golonka *et al.*, 2018, 2019, 2024, 2025; Marzec *et al.*, 2020). The PKB has a very complicated geological structure, commonly called a mélange (Fig. 1). It was formed as a mixture of elements that had a different lithology and differed in age, as a result of tectonic and sedimentation processes (Golonka *et al.*, 2017, 2018).

The sedimentation processes started with the origin of the Alpine Tethys during Jurassic times. The Złatne and Magura basins were parts of the Alpine Tethys, separated by uplift of the Czorsztyn Ridge. Carbonate sedimentation predominated in these basins and on the ridge. The sedimentation of synorogenic clastics was associated with subduction and the origin of an accretionary prism that started at the southern margin of the Alpine Tethys during the Albian. This accretionary prism reached the Czorsztyn Ridge at the end of the Late Cretaceous. The overriding of this ridge contributed to the formation of olistoliths in the northern Magura basin (Waśkowska and Golonka, 2024, 2025). The clastic material was deposited in both the Złatne and Magura basins during Late Cretaceous–Neogene times. The tectonic processes contributed to the formation of the present-day PKB structure.

The Złatne, Branisko and Hulina units were distinguished within the investigated area (Golonka *et al.*, 2024, 2025). The Złatne Unit contains rocks deposited in the Złatne Basin, the Hulina Unit contains rocks deposited in the Magura Basin, and the Branisko Unit contains rocks deposited on the slope of the Czorsztyn Ridge. The basins were separated by the Czorsztyn ridge and took the form of olistostromes with olistoliths. The belt of olistoliths ("block-in-matrix" zone) was formed along the southern margin of the Magura Basin and is now located within the Hulina Unit. The olistoliths represent rocks, associated with the Czorsztyn Ridge (Waśkowska and Golonka, 2024, 2025). The Złatne Unit is in contact with the Central Carpathian Paleogene, belonging to the Central Carpathian Plate (Golonka *et al.*, 2024, 2025).

Tectonic processes were primarily associated with the occurrence of continuous and discontinuous deformations, such as the formation of fault zones, block movement, folding, and uplifting. They occurred mainly within the Złatne, Branisko, and Hulina units, originally formed during the Late Cretaceous Epoch. They were transformed again in the Neogene period and are now a mosaic of tectonic elements, often heavily deformed and fragmented (Golonka *et al.*, 2024, 2025; Waśkowska and Golonka, 2024, 2025; Fig. 1).

Geophysical research covered the area of the olistolith belt and its complex surroundings.

MATERIALS AND METHODS

Geophysical research was conducted in South Poland in the vicinity of Krempachy and Dursztyn villages, near the Korowa Skała rock formation. These studies were especially focused on the identification of the mélange zone of the Pieniny Klippen Belt. This zone has a W–E trend and the geophysical survey was performed in a perpendicular direction. Therefore, geophysical observations were made along the profile, presented in Figure 2, with an almost S–N direction. For all three methods, the profile has a length of 1 km, but with a slight offset for each other, which did not affect the quality of the interpretation of the complex.

One of the geophysical methods used in this research was the gravity method. According to Newton's universal gravitational laws, the value of the gravity field depends especially on the mass distribution within the Earth. The gravity method is based on observations of the small variation in the natural gravity field of the Earth. These changes are connected with the density distribution of the rock mass and are presented as the distribution of Bouguer anomalies. These anomalies are most often related to geological or anthropogenic structures. Therefore, this method is mainly used to map the geological basement and geological structures in the Earth's crust and, in the same way, to investigate natural or anthropogenic voids and unconsolidated zones.

For geoelectrical research, the electrical resistivity tomography (ERT) method was applied. ERT (Dahlin, 1996, 2001), originally resistivity imaging (RI), is currently the most popular surface geoelectrical method applied for detailed electrical resistivity studies. It is widely used, including in geological and geomorphological studies (e.g., Chambers *et al.*, 2012; Metwaly and AlFouzan, 2013; Nur Amalina *et al.*, 2017; Woźniak *et al.*, 2018; Akinbiyi *et al.*, 2019; Woźniak and Bania, 2019a, b; Bania and Woźniak, 2022; Bania *et al.*, 2024).

For seismic research, seismic refraction tomography (SRT) was used. SRT is a geophysical technique that allows the determination of the elastic properties of the soil and rock medium. This method is non-invasive and allows for the investigation of geological units occurring in subsurface structures. The aim of SRT investigations is to obtain a two-dimensional model of seismic wave velocities in the geological medium. The SRT method is commonly used, for example, to determine shallow geological structure (Avalos *et al.*, 2016; Cichostępski *et al.*, 2024), determine groundwater levels (Grelle and Guadagno, 2009), investigate landslides (Zainal *et al.*, 2021) and assess rippability (Ismail *et al.*, 2010). The SRT measurement is a kind of supplement to the deep reflection seismic studies, conducted in 2015 in the Pieniny Klippen Belt area (Golonka *et al.*, 2019; Marzec *et al.*, 2020), because owing to the methodology of conducting this type of studies, the shallow zone is not imaged.

Acquisition and processing of gravity data

The gravity survey was carried out along the G1 profile, about 1 km long and extending in a SSW–NNE direction. The distance between the gravity observation stations was 10 m.

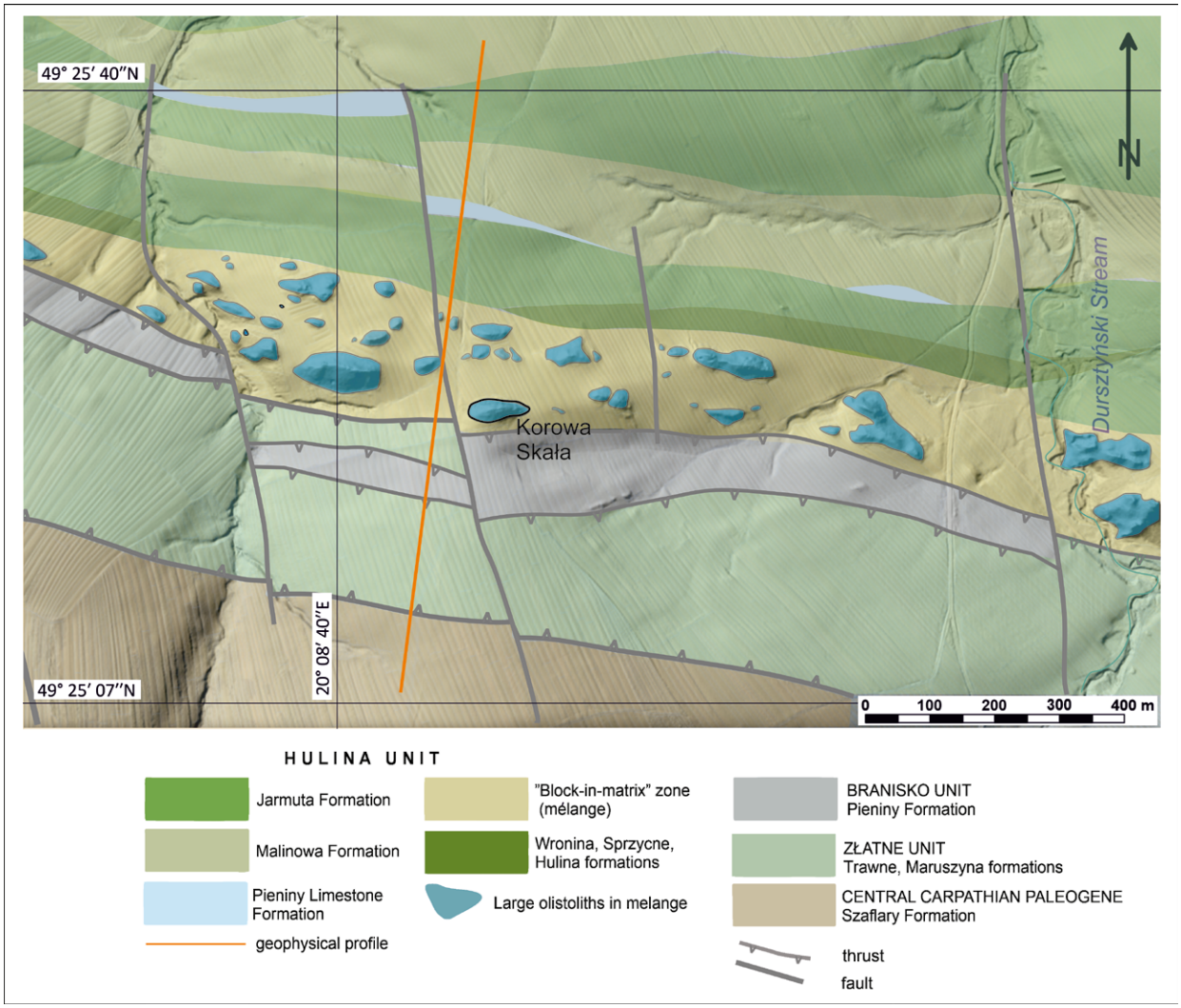

Fig. 1. The PKB geology in the geophysical research area. Modified after Golonka *et al.*, 2025.

Gravity observation was done using the Autograv CG-5 Scintrex Gravimeter, an instrument that is used to measure relative gravity values. All gravity observations along the survey profile were performed with a special measurement system, consisting of performing gravity observations in an independent closed loop, where the first- and the last-loop observations were done in a reference (drift) base station. The gauge of the accuracy of the gravity observations was the mean square error of a single measurement. To evaluate the gravity survey, gravity observations are repeated on at least 5–10% stations. If this gravity survey is performed with high quality, it can be processed to obtain the Bouguer anomaly (Dg_B).

The law of gravity shows that the gravity value depends on the distance from the geological source that causes it. The topography of the Earth's surface is very variable, so the gravity observation stations are on different levels (elevations). In that case, gravity research cannot be done without a geodetic survey. Geodetic activities included determining the location and elevation above sea level of the observation stations, using GPS and tachometric measurements.

The Bouguer anomalies can be calculated only when the influence of terrain elevation values is removed from gravity observations. Bouguer reduction was used to remove this effect (influence). It means that the values of three corrections – free-air correction, Bouguer correction, and terrain correction – were added to gravity observations (Telford *et al.*, 1990a; Porzucek and Loj, 2021).

It is necessary to determine a value of the average rock mass density in order to calculate Bouguer and a good-quality terrain correction. The gravity survey was carried out in the area, where the PKB, Podhale flysch, and Magura Nappe boundary are located. Therefore, the determination of the density, based on archival data, was difficult. For this reason, it was decided to use special gravity methods to determine this density (in situ). After calculations, it was determined that the average density in the research area was 2.51 g/cm^{-3} (Łój *et al.*, 2024).

The Bouguer anomaly was calculated as the difference between the gravity observation value with Bouguer reduction and the latitude correction (normal gravity value). The latitude correction was calculated on the basis of the International Gravity Formula for the Earth model of the Geodetic Reference System 1980 (Moritz, 2000).

The Bouguer anomaly reflects the distribution of the density (mass) of geological structures. The anomaly value at

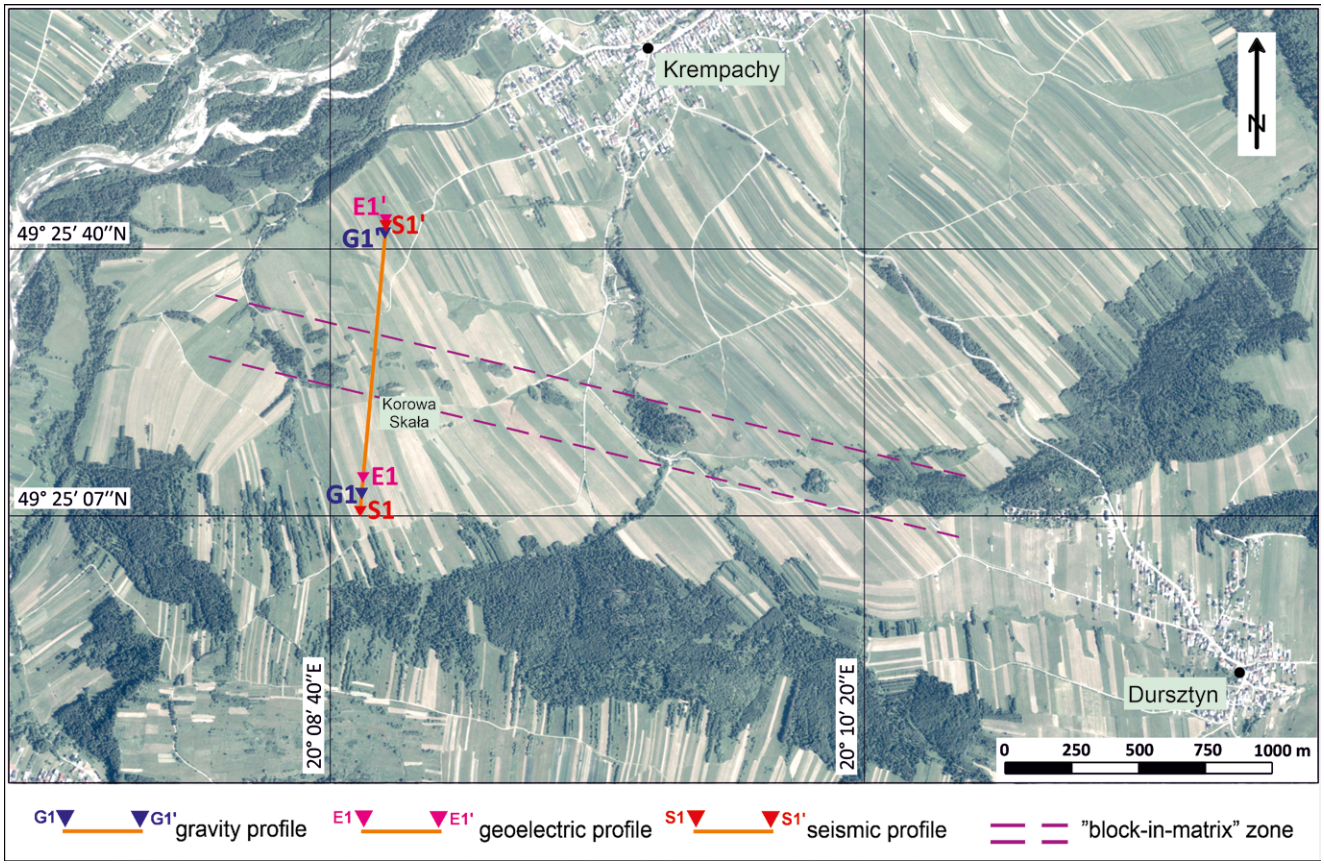

Fig. 2. Location of the geophysical research profile (acc. to: *www.geoportal.gov.pl/pl/dane/ortofotomapa-orto/*).

each observation point depends on the mass distribution below and around this point, and for this reason, anomalies can be divided into components that can be connected with the size and depth of the sources. The anomalies connected with deep sources are named regional and associated with shallow sources, namely, residuals (local).

All Bouguer anomalies can be described on the basis of their amplitude and horizontal range. These attributes can be identified as an anomaly frequency (Fajklewicz, 2007). From this point of view, it is possible to use frequency filters to interpret the gravity data. It can be carried out using the Fourier transformation. This approach has been known since the 1950s (Dean, 1958; Swartz, 1954) and was successively developed (Bhattacharyya, 1966, 1967; Darby and Davies, 1967; Gunn, 1975). It means that it is possible to use wavelength (wavenumber) filters to divide the Bouguer anomalies into regional and residual components.

During the interpretation of gravity data, Butterworth and Gauss low-pass and high-pass filters were used. The low-pass filter (passes the low-frequency signal) was used to calculate the regional anomaly, connected with deep sources, and the high-pass filter to calculate residual anomalies, connected with small shallow sources.

ERT Data Acquisition and processing

2D ERT measurements were performed on survey line P01, 975 m long (Bania *et al.*, 2024; Golonka *et al.*, 2024). The P01 profile was orientated approximately perpendicular to the "block-in-matrix" zone orientation. This location relative to the "block-in-matrix" zone was intended to best meet the measurement and interpretation conditions for the 2D ERT variant. Measurements were made with a SuperSting R8/IP/SP system (AGI – Advanced Geosciences, Inc.) and a set of 112 electrodes. The electrodes were placed at a 5 m spacing. The initial section of the planned profile was 555 m long. Using the roll-along technique, the measurement was continued by extending the profile by repeatedly moving the appropriate sections of the 8-part measuring cable so that the final length of the survey line was approximately 1 km. The measurement line covered the expected width of the "block-in-matrix" zone with appropriately large overlaps. The amount of data recorded for this profile was 12,086 apparent resistivity values. Such a large amount of data resulted from the use of a specially developed measurement scheme, using Multiple Gradient Arrays (Dahlin and Zhou, 2004; Loke, 2012). This approach provided high-density and high-resolution data. At the same time, gradient arrays were selected to maintain the AB/MN = 10 relation for all sizes of the current AB dipole, which ensured an appropriately high "signal" level.

Conducting electrical resistivity tomography measurements requires knowledge of the morphology of the terrain surface along the survey line (see e.g., Fox *et al.*, 1980; Lu *et al.*, 2015). In practice, this means that the position of the electrodes must be levelled. In the discussed case, to limit the scope of geodetic field work, appropriate, commonly available for Poland, topographical data (XYZ) in the

form of a digital elevation model (DEM) was applied. This model is represented in the form of a rectangular grid with a mesh size of 1 m × 1 m (*www.geoportal.gov.pl/dane/numeryczny-model-terenu.*). Therefore, geodetic field work for the ERT studies was limited to determining the position of selected points on the P01 profile with the GNSS receiver. The accuracy of the applied method is completely sufficient, especially considering the scale and objectives of the ERT measurements.

ERT Data inversion

In geophysical interpretation, two basic stages can be distinguished: quantitative interpretation of data and contextual interpretation, that is, description of the results of geophysical interpretation in geological categories, taking into account the purpose of the research.

One of the latest versions of Res2Dinvx64 software (ver. 4.10.21; Aarhus Geosoftware; Loke, 2012) was applied for the new variant of quantitative interpretation of 2D ERT data. This software allows for the modification of numerous parameters (or procedures) to control the numerical iterative inversion process. Each of these parameters (or procedures) affects the final result of the interpretation to a varying extent. It should be noted that the inversion result is inherently ambiguous (from the mathematical and physical perspective) even for an ideal 2D situation.

The basic step in the Res2Dinvx64 software is the selection of the inversion method. Most often, this comes down to applying one of the two main variants: blocky (robust; L_1-norm) inversion or smoothness-constrained (L_2-norm) inversion, which use different definitions of the inversion error (e.g., Loke *et al.*, 2003). To obtain greater details of the geological setting in the near-surface zone, which was intended to isolate a larger number of high-resistivity structures (olistoliths?), as well as a more accurate comparison to the anomaly distribution obtained by the gravity method, a specific set of other inversion parameters was applied. These parameters are identical to those used by Woźniak and Bania (2019a). After inversion, an analysis of the distribution of inversion errors (which are related to the impossibility of matching the theoretical 2D model with the measurement data) was carried out, using the "RMS error statistics" option. From the entire dataset, those for which an individual error exceeded 12% were removed. The filtered data were subjected to reinversion with a previously selected set of parameters. The result of the last inversion iteration, with the absolute error achieved at a level of 1.00%, was treated as the final model. Then, the obtained result data were visualized in the form of an inverse model resistivity section.

Acquisition and processing of seismic data

Seismic refraction tomography uses artificially generated seismic waves that propagate through the subsurface. The propagation velocity of seismic waves varies and depends on the parameters of the medium, such as lithological composition, structure, texture, rock framework, porosity, fracturing, and degree of weathering (Adelinet *et al.*, 2018). The velocity of the seismic wave is related to the hardness (strength) of the material. Generally, the harder the rock, the higher the velocity of the seismic wave (Olona *et al.*, 2010). Knowledge of the geology of the study area and the obtained distribution of seismic wave velocities provide the possibility of determining the subsurface structure, the thickness of the weathered zone, and the type and depth of the rock basement.

Seismic refraction tomography is based on the arrival times of seismic waves that were critically refracted at the interface between layers characterized by different velocities. The travel times of seismic waves (first arrivals of direct and refracted waves) are recorded by receivers (geophones), placed in a straight line along the measurement profile. From multiple recordings, using a combination of shot points and receiver points, a set of travel times can be obtained. The geophysical procedure of tomographic inversion of the travel time dataset allows obtaining a velocity model of the subsurface (Zhang and Toksöz, 1998), providing good resolution, even in the case of a complex geological structure (Sheehan *et al.*, 2005). The depth of investigation is usually between 0.3 and 0.5 times the active spread length.

Seismic data were measured, using three Geode seismographs (Geometrics) and 14 Hz vertical geophones, spaced at 5 m intervals. The active spread contained 72 geophones, corresponding to a measurement length of 355 m. The profile was measured in sections with 115 m overlaps (roll-along technique). The measured profile had a length of 1075 m. A Gisco ESS-500 Turbo weight drop was used as the seismic wave source (weight drop of 227 kg mass). The first shot point was located 2.5 m from the first geophone and then the seismic wave was generated every 30 m. To achieve a high signal-to-noise ratio, up to three shots were made at each shot point and then summed. The data obtained are of very good quality.

The first step in the processing of seismic refraction data is the manual picking of the first arrivals of the compressional wave on each recorded seismic record. On the prepared travel time sets, the seismic inversion procedure was applied using the tomographic algorithm of the shortest path ray tracing. This method utilizes an initial velocity model, which is then iteratively modified (in terms of vertical and horizontal velocity distributions), where during each iteration the theoretical travel times generated based on the given model are compared with the actual travel times. This process continues until the difference between theoretical and interpreted travel times is minimized (Zhang and Toksöz, 1998; Sheehan *et al.*, 2005). The initial model for inversion was built, using a gradient increase in velocity with depth. The model parameters ranged from 550 m/s to 5,000 m/s. The inversion process was stopped after 10 iterations, when it reached an RMS (root mean square) error of 1.2%. The velocity model obtained was trimmed in areas, where there was no ray coverage. With the applied methodology, the maximum depth of subsurface seismic imaging was 80–100 m.

RESULTS OF GEOPHYSICAL RESEARCH

The geophysical observations have been subjected to processing, according to the principles described above. This allowed the use of interpretation procedures, and their results are described below.

Gravity results

The gravity interpretation was carried out on the basis of Bouguer anomalies. These anomalies were calculated by taking into account the previously determined average density value. There was no correlation between the Bouguer anomalies and the terrain shape along the profile, so this means that the average density value estimation was accurate and the Bouguer reduction was calculated correctly.

No doubt, the observation gravity value included measurement error as well as high frequency noise, which was connected with near-surface density changes. The low-pass frequency filter, the Butterworth filter, for the 50 m wavenumber cut-off value was used to remove the measurement errors and noise from the observation values. The Bouguer anomaly distribution without any disturbances is presented in Figure 3.

The amplitude of the anomaly along the profile was high and approached 17.5 μ/s^{-2} and along the profile the general changes were visible. First, from the south the value of Bouguer anomalies decreased, and they had minimum near 750 m of profile, and next, in a northerly direction, those values start to increase. This direction of anomaly changes should be connected with the thickness of flysch sequences of the Podhale Flysch Basin. There was geological contact between the Podhale Flysch Basin and the Pieniny Klippen Belt in this part of the profile, but there were no visible changes in the Bouguer anomalies. So, it can be argued that there had not been any contrast between the density value of both structures and that this density is close to 2.51 g/cm^{-3}.

The distribution of Bouguer anomalies can be divided into four zones (Fig. 3) with a different anomaly character. The part of the Bouguer anomaly distribution, where the fastest value change was visible, was divided into two zones, zone G-I and zone G-II. This division was determined by the different nature of the distribution. While in zone G-I the distribution was smooth, but with a significant horizontal gradient, in zone G-II the horizontal gradient of the distribution was smaller, and some local fluctuations appeared. The "block-in-matrix" zone, with rocks visible at the ground surface, was located in the part of zone G-II, but in Bouguer the distribution of the anomalies was almost invisible. In the next G-III zone, the anomaly distribution had a good visible relative negative nature, which is most probably associated with a geological zone of lower density than in its southern surroundings, but also in relation to the northern side, where the value of Bouguer anomalies increased again, making zone G-IV.

The sufficiently dense measurement step (10 m) along the profile allowed recording smaller, more local anomalies. This type of anomaly is associated with small, shallow, local geological structures, such as olistoliths, which are of particular interest in this geophysical research. The problem was that the low amplitude of these anomalies in relation to the amplitude of the complete Bouguer distribution made their interpretation difficult. Therefore, to better identify them, the authors removed the regional trend from the Bouguer anomaly values using the Gauss filter as the isolation filter. Analysis of several wavenumber cutoff values showed that the best wavenumber cutoff value was 300 m. After this, the residual anomalies were calculated as the best approximation of the local anomalies (Fig. 4).

Along the profile, several residual anomalies appeared with small amplitudes and a reduced horizontal range. These small positive and negative anomalies could be related to small changes in density in the shallow part of the rock mass. Therefore, the first smooth zone G-I could be divided into three subzones: two zones with a positive value of residual anomalies, separated by a negative residual anomaly G-Ia. It means that there is a shallow geological layer with a smaller density, surrounded by layers with a higher density. Zone G-II was non-uniform in nature as well; the detailed

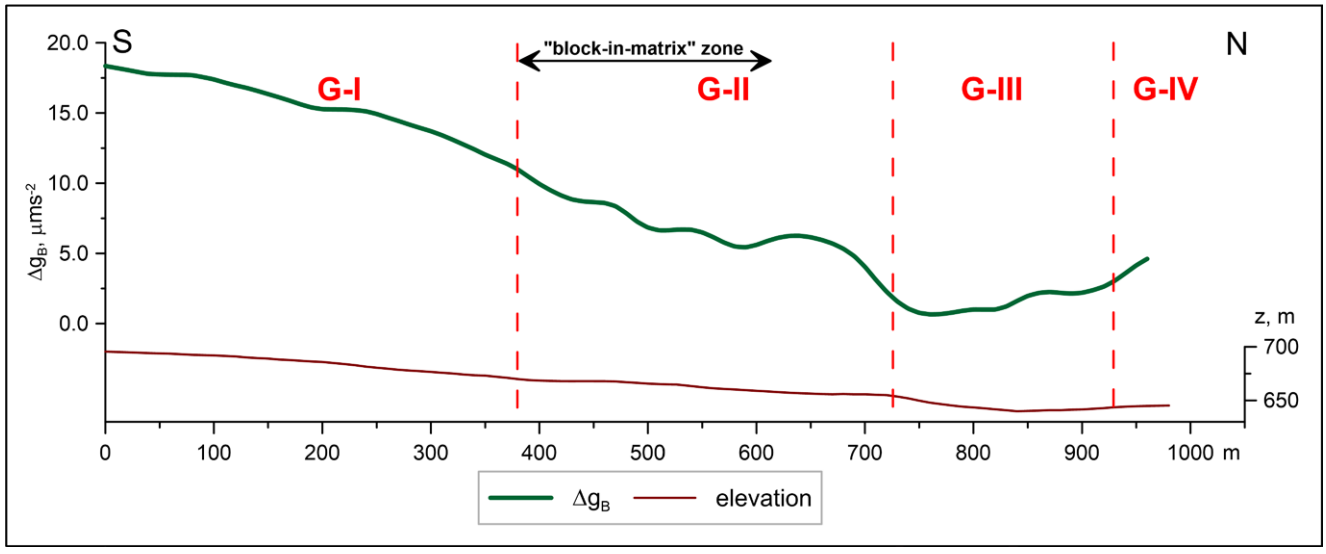

Fig. 3. The Bouguer anomalies distribution Dg_B along the profile.

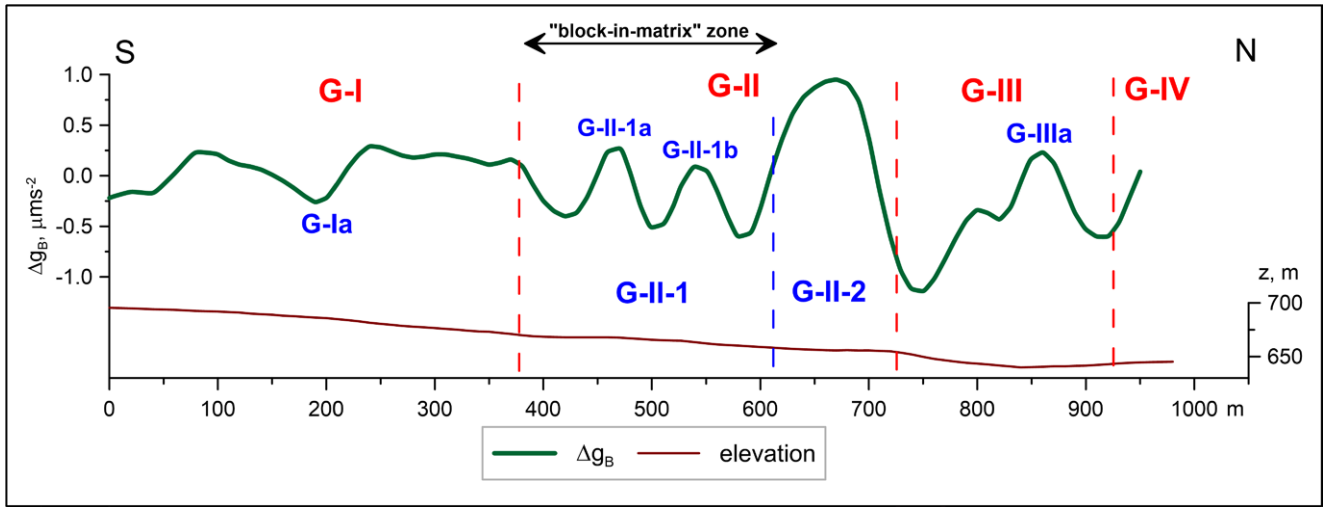

Fig. 4. The distribution of residual anomalies along the profile.

analysis of the residual anomalies distribution in this zone allowed the division of it into two subzones: G-II-1 and G-II-2. The first one generally had a negative nature of residual anomaly, but with two small positive anomalies, G-II-1a and G-II-1b, visible inside. There was only one large-amplitude residual anomaly in the second subzone of zone G-II. In gravity research, limestone olistoliths should appear as relatively positive Bouguer anomalies and positive residual anomalies, so the visible anomalies G-II-1a and G-II-1b were of a suitable nature. Furthermore, these anomalies were very closely correlated with the limestone rocks that protruded above the surface near the gravity profile. So, it is very probable that these anomalies are associated with the same type of limestone, located below the ground surface. From this point of view, the first subzone of zone G-II can be described as a low-density layer with individually separated limestone blocks (high density); therefore, this confirms the assumption that the visible rocks are olistoliths.

To the north of zone G-II (Fig. 4), the anomalies with a small horizontal range were no longer observed; only in zone G-III the positive residual anomaly G-IIIa appeared, indicating the existence of the higher density layer.

ERT Results

The result of the quantitative interpretation of the ERT P01 profile in the form of an inverse model resistivity section clearly shows six zones in the geological setting (Fig. 5).

From the southern side to about 250 m of the cross-section, the first zone E-I is visible as a layered structure. It consists of high (80–300 Ωm) and low-resistivity (10–20 Ωm) structures located close to the surface, and below it there is

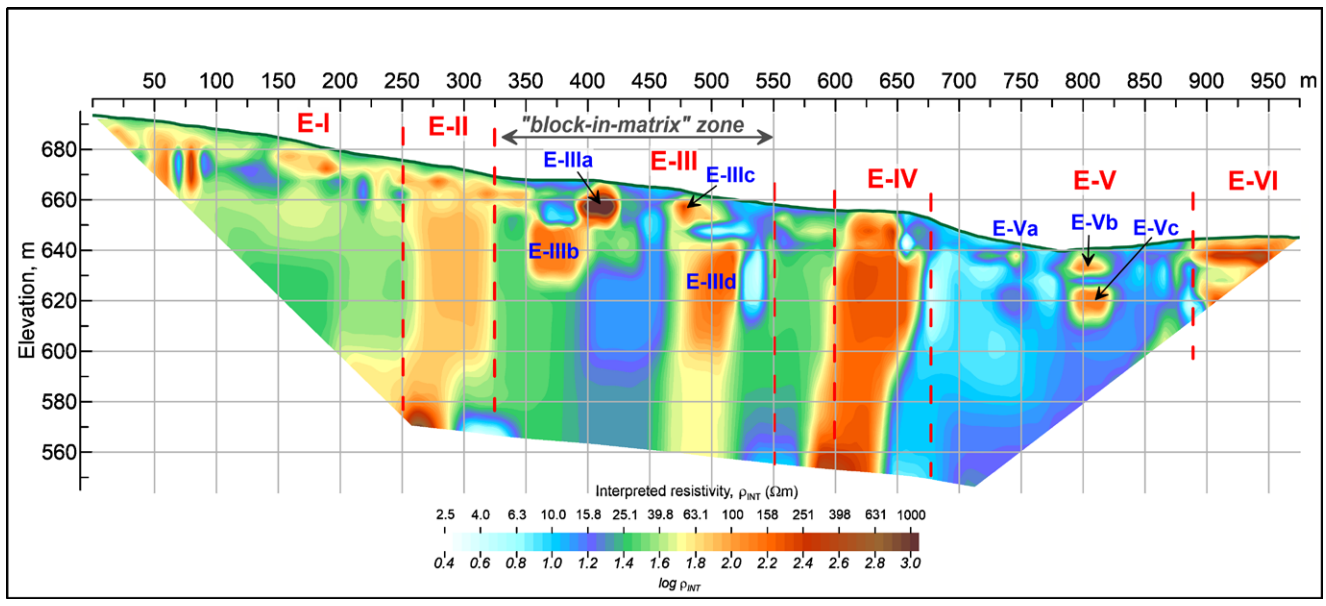

Fig. 5. Inverse model resistivity section for ERT P01 survey line.

a medium with a resistivity of about 40 Ωm. Furthermore, on the profile is a visible high-resistivity zone E-II (resistivity 60–100 Ωm), the monolithic nature of which clearly differs from the structure of the "block-in-matrix" zone. In the "block-in-matrix" zone E-III, local high-resistivity anomalies (>150 Ωm), and accompanying low-resistivity anomalies (<25 Ωm) are visible. The location of high-resistivity structures correlates in places with limestone rocks, visible at the surface. Compared to the interpretation variant obtained earlier (Bania *et al.,* 2024), instead of the Ol structure, two separate structures were obtained in the inversion process: E-IIIa and E-IIIb. It should be noted that structure E-IIIa, owing to its relatively high interpreted resistivity (>800 Ωm), compared to the remaining structures E-IIIb, E-IIIc, and E-IIId (approximately 150–200 Ωm), will most likely be associated with the close proximity of the limestone block, which protrudes from the surface (Fig. 5). Such a high value of the interpreted resistivity may be caused by the 3D effect of the blocks (cf. Sjödahl *et al.,* 2006; Bania and Ćwiklik, 2013). It is difficult to assess whether the E-IIIb structure is an independent structure or is somehow related to the E-IIIa structure. Generally, in geological terms, E-IIIa-b structures could be olistoliths, which are embedded in a low-resistivity matrix, composed to a large extent of clay.

The next distinctive zone E-IV is dominated by a slightly northward inclined monolithic high-resistivity structure (100–300 Ωm). Further north, the authors observe a rapid change of the medium, a low-resistivity (<20 Ωm) zone E-V, in which several high-resistivity structures (approximately 150 Ωm) are visible, the first E-Va at 750 m, and two E-Vb and E-Vc (one above the other) in the centre at 810 m. In the northernmost part of the cross-section is visible the high-resistivity formation E-VI (approximately 100–450 Ωm).

Seismic results

The velocity of seismic waves depends on the type of rocks and the degree of their diagenesis. Lower velocities may indicate the presence of poorly consolidated or weathered rocks with a low degree of diagenesis, such as mudstones, marls, and soil, while higher velocities may indicate hard rock, such as sandstones and limestones (Yilmaz, 2001). The obtained SRT section showed significant horizontal and vertical variations in seismic P-wave velocity from 1,500 m/s to 4,000 m/s, showing strong lateral contrasts in subsurface properties (Fig. 6), which revealed the complex structure of the studied area. On the basis of the velocity distribution, the profile was divided into five zones marked in Figure 6.

The lowest velocities (up to 1,500 m/s) correspond to a soil layer that is about 2 m thick, and below it a high horizontal velocity variability is observed. The profile begins with a high velocity (up to 3,300 m/s), which dips steeply towards north, and it is the south boundary of zone S-I. The zone is divided with a horizontal velocity boundary at a depth of 90 m into two parts: a shallower layer with moderate velocity (2,900 m/s) and a deeper layer with velocity of 3,100 m/s. In the shallower layer, near the surface, two areas of low velocity (2,000 m/s) are visible.

The next highlighted zone S-II points to a massive structure with the highest velocity (up to 4,000 m/s). The following zone S-III contains several high- and moderate-velocity areas, which are bounded by low-velocities. The authors observed a high velocity (3,500 m/s) rounded structure S-IIIa and two moderate velocity areas S-IIIb and S-IIIc (2,800–2,900 m/s). The S-IIIa structure and the S-IIIb area occur within the "block-in-matrix" zone. At the location of the S-IIIa structure, just a few metres from the profile, there is a limestone outcrop. This convergence allowed identifying the structure as limestone, probably an olistolith embedded in a low velocity medium such as mudstone or weathered sandstone. Below highlighted structure and areas the authors observe rocks with higher velocity (3,300 m/s).

The S-IV zone has generally lower velocities, 2,000 m/s for the shallower part, and 2,700 m/s for the deeper part. Within this low velocity part, a small structure S-IVa of slight increase in velocity can be observed at 850 m of the profile and another structure S-IVb with higher moderate velocity (2,800 m/s). The zone S-V describes a high velocity layer (up to 3,800 m/s), which rises steeply towards the south.

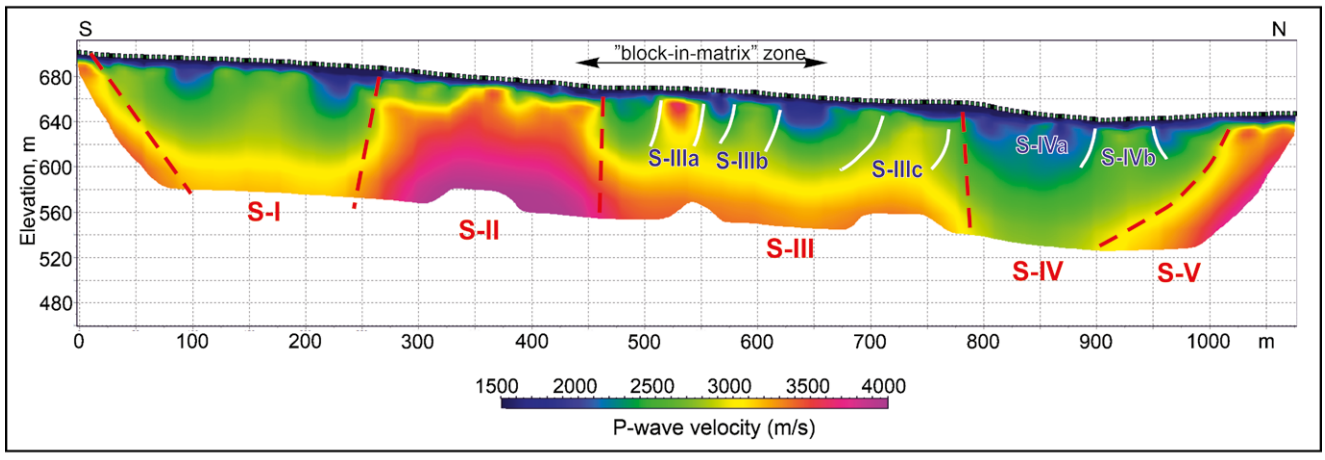

Fig. 6. The results of seismic refraction tomography along the profile. Dashed lines – main seismic boundaries.

DISCUSSION

Geophysical research was carried out using three geophysical methods (gravity, ERT, and SRT) along a profile, running perpendicular to the boundaries of the mélange structures of the PKB (Figs 1, 2). The purpose of the study was to identify the melange zone of the PKB and, in particular, to test the hypothesis that the "block-in-matrix" zone consists of a group of separate limestone blocks distributed in the zone as "raisins in a cake". Using different geophysical methods, the authors obtained a description of the same geological site, based on different physical parameters of the geological structures. The use of the gravity method allowed the authors to follow the changes in mass (density) distribution in the rock formations, which are observed in the form of gravity anomalies. The ERT method uses the variable resistivity of rock formations to identify geological structures. However, the basis of the SRT method is the fact that seismic waves propagate at different speeds in different formations.

Therefore, it is logical that the results of the research may differ to some extent from each other. However, what is more important is that despite the trace of different physical parameters, the research results obtained clearly indicate zones corresponding to the same geological structures. An integrated interpretation of the results of the various geophysical methods showed that several of such compatible zones can be identified along the profile (Fig. 7).

In the first common A-B zone, an increase in gravity values and seismic wave velocity was observed. On the southern side, this zone can be linked to the direction of the boundary between the Złatne and the Branisko units, while its northern boundary was the contact of the Branisko Unit and the "block-in-matrix" zone. The increase in the values of the physical parameters was related to the fact that the Branisko Unit is mainly composed of limestone. While for gravity and seismic methods, this zone appears to be fairly homogeneous in terms of the distribution of physical parameters, the ERT method shows variations within it, with a strongly defined resistivity boundary from 380 m of the cross-section.

The next zone B-C was also observed by all three methods, and the reduction in physical parameters tracked by all of them indicates that it may correspond to weakly compacted siltstone or marl-type rocks. However, two anomalies, "1" (centre about 530 m) and "2" (centre about 600 m), with high values of density, resistivity, and seismic wave velocity, are strongly defined. By analysing the direction of the profile on the ground surface and on the geological map (Figs 1, 2), it can be seen that in these anomalous areas the profile runs close to limestone rocks protruding at the surface. Seismic and geoelectric studies clearly indicate that these rocks have limited vertical dimensions. The nature of the observed changes in physical parameters leads to the conclusion that these structures are separate, unconnected blocks of rock stuck in the surrounding rocks, like "raisins in a cake", therefore, one can conclude that the observed changes are associated with sedimentary-type olistolith blocks.

Further north, another D-E zone, common to all methods, appears and is located within the Jarmuta Formation. The distribution of gravity anomalies and of interpreted resistivity sections is marked by a very strong increase in the values of the physical parameters, while the distribution of velocity also shows a weaker increase. It is also worth noting that the maximum of the gravity anomaly is shifted southward, relative to the maxima of the resistivity and wave velocity values in the other methods. This is due to the fact that the structure that generates these distributions is tilted towards the south. On the basis of the properties of the physical parameters, it should be inferred that this structure is composed of compact formations, probably sandstones.

Subsequently, from 780 m until almost the end of the profile, an E-F zone of reduced density, resistivity, and seismic-wave velocity appears within similar limits for all methods, most probably associated with the Jarmuta and Malinowa formations. In the distributions of results from all methods, a small anomaly "3" (approximately centred at 925 m) can be seen within this zone, clearly marked by gravity and ERT methods, and somewhat weaker by seismic. The increase in the values of the physical parameters for all methods indicates that the formations in this zone are hard rocks, and analysis of the geological map reveals that a belt of Jurassic limestone appears to the north of the profile. Thus, it is possible that these formations are present in the anomalous area, but in the form of a small lens or block, not visible on the ground surface. Toward the end of the profile, from about 1,010 m, an increase in the physical parameter values for all methods is again marked, but owing to limited geophysical data, it is difficult to clearly identify the source of these changes.

In addition to interpreting the shallow part of the subsurface, geophysical methods also allow inferences to be made about the deeper structure; however, owing to the burden of greater interpretation error, the results obtained are not always fully compatible. In the case of the distribution of gravity anomalies, by analysing the regional trend of Bouguer anomalies distribution, it can be concluded that this reflects a northward sinking of the crystalline basement and thus an increase in the thickness of the flysch rocks.

CONCLUSIONS

The use of three geophysical methods provided information on the geological structure along the research profile, on the basis of different physical properties of the rocks: bulk density, resistivity, and seismic P-wave velocity. The correlation between them is not regular, i.e., an increase (decrease) in one property does not always correspond to an increase (decrease) in another property. In the investigated profile, the compatibility of changes in physical properties was very high, and therefore the reliability of the geophysical interpretation is also very high. Therefore, it should be assumed that rocks projecting above the ground surface in the "block-in-matrix" zone have relatively limited dimensions. They should be identified as olistolithic-type rock blocks. In addition, the geophysical survey has very well reflected the position of the boundaries between the different formations, crossed by the profile.

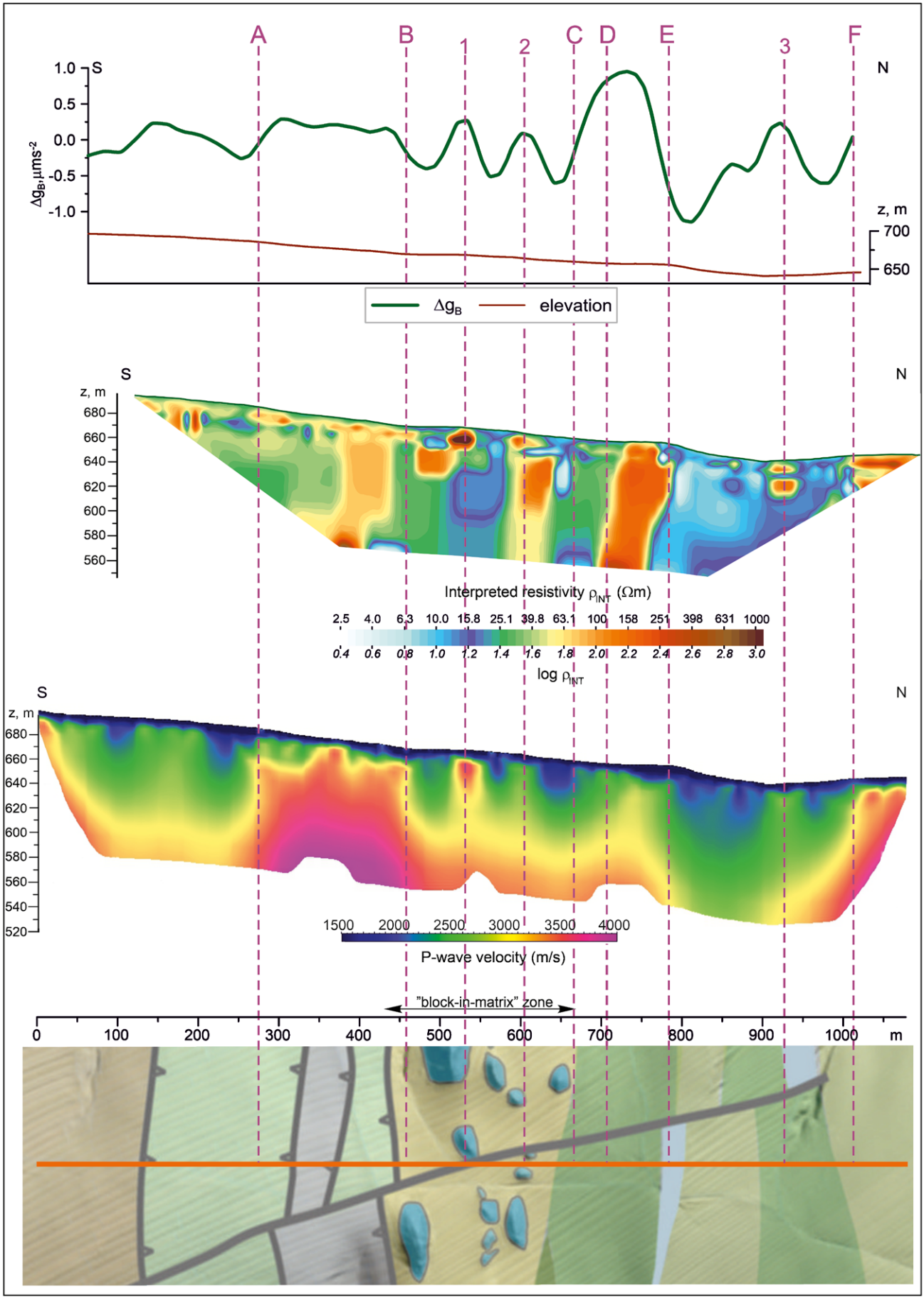

Fig. 7. The results of geophysical research (sequentially from the top: gravity, the ERT, the SRT methods) along the profile shown on the geological map (description as in Figure 1).

Acknowledgments

This research was financially supported by the Polish National Science Centre Grant NCN-2019/35/B/ST10/00241 and by the AGH University of Krakow Statutory Research Project no. 16.16.140.315. We are grateful to anonymous reviewers for their valuable remarks.

REFERENCES

Adelinet, M., Domínguez, C., Fortin, J. & Violette, S., 2018. Seismic-refraction field experiments on Galapagos Islands: A quantitative tool for hydrogeology. *Journal of Applied Geophysics*, 148: 139–151.

Akinbiyi, O. A., Oladunjoye, M. A., Sanuade, O. A. & Oyedeji, O., 2019. Geophysical characterization and hydraulic properties of unconsolidated floodplain aquifer system in Wamako area, Sokoto State, north-western Nigeria. *Applied Water Science*, 9, article no. 177.

Avalos, E. B., Malone, D. H., Peterson, E. W., Anderson, W. P. & Gehrels, R. W., 2016. Two-dimensional seismic refraction tomography of a buried bedrock valley at Hallsands beach, Devon, United Kingdom. *Environmental Geoscience*, 23: 179–193.

Bania, G. & Ćwiklik, M., 2013. 2D Electrical Resistivity Tomography interpretation ambiguity – example of field studies supported with analogue and numerical modelling. *Geology, Geophysics & Environment*, 39: 331–339.

Bania, G. & Mościcki, W. J., 2024b. Rozpoznanie płytkiej struktury pienińskiego pasa skałkowego z wykorzystaniem sejsmicznej tomografii refrakcyjnej. In: Golonka, J., Łój, M. & Waśkowska, A. (eds), *Geofizyczne odwzorowanie melanży w płytkich strefach pasm orogenicznych – przykład z pienińskiego pasa skałkowego*. Wydawnictwa AGH, Kraków, pp. 95–127. [In Polish.]

Bania, G., Mościcki, W. J. & Golonka, J., 2024. ERT field survey supported with numerical and analogue modeling applied to study a fragment of the Pieniny Klippen Belt (Spisz Pieniny Mountains, southern Poland). *Geological Quarterly*, 68, 22.

Bania, G. & Woźniak, T., 2022. Subsurface imaging of fluvial deposits of the Wisła River valley in Kraków (southern Poland) by 2D ERT survey. *Geological Quarterly*, 66, 23.

Bhattacharyya, B. K., 1966. Continuous spectrum of the total magnetic field anomaly due to a rectangular prismatic body. *Geophysics*, 31: 97–121.

Bhattacharyya, B. K., 1967. Some general properties of potential fields in space and frequency domain, A review. *Geoexploration*, 5: 127–143.

Chambers, J. E., Wilkinson, P. B., Wardrop, D., Hameed, A., Hill, I., Jeffrey, C., Loke, M. H., Meldrum, P. I., Kuras, O., Cave, M. & Gunn, D. A., 2012. Bedrock detection beneath river terrace deposits using three-dimensional electrical resistivity tomography. *Geomorphology*, 177–178: 7–25.

Cichostępski, K. & Dec, J., 2024b. Rozpoznanie płytkiej struktury pienińskiego pasa skałkowego z wykorzystaniem sejsmicznej tomografii refrakcyjnej. In: Golonka, J., Łój, M. & Waśkowska, A. (eds), *Geofizyczne odwzorowanie melanży w płytkich strefach pasm orogenicznych – przykład z pienińskiego pasa skałkowego.* Wydawnictwa AGH, Kraków, pp. 129–150. [In Polish.]

Cichostępski, K., Dec, J., Golonka, J. & Waśkowska, 2024a. Shallow seismic refraction tomography images from the Pieniny Klippen Belt (southern Poland). *Minerals*, 14: 155.

Dahlin, T., 1996. 2D resistivity surveying for environmental and engineering applications. *First Break*, 14: 275–283.

Dahlin, T., 2001. The development of electrical imaging techniques. *Computers and Geosciences*, 27: 1019–1029.

Dahlin, T. & Zhou, B., 2004. A numerical comparison of 2D resistivity imaging with ten electrode arrays. *Geophysical Prospecting*, 52: 379–398.

Darby, E. K. & Davies, E. B., 1967. The analysis and design of two-dimensional filters for two-dimensional data. *Geophysical Prospecting*, 15: 383–406.

Dean, W. C., 1958. Frequency analysis for gravity and magnetic interpretation. *Geophysics*, 23: 97–127.

Fajklewicz, Z., 2007. *Grawimetria stosowana*. Uczelniane Wydawnictwa Naukowo-Dydaktyczne AGH, Kraków, p p. 347–372. [In Polish.]

Fox, R. C., Hohmann, G. W., Killpack, T. J. & Rijo, L., 1980. Topographic effects in resistivity and induced polarization surveys. *Geophysics*, 45: 75–93.

Golonka, J., Chowaniec, J. & Waśkowska, A., 2024. Zarys budowy geologicznej zachodniej części pienińskiego pasa skałkowego w Polsce. In: Golonka, J., Łój, M. & Waśkowska, A. (eds), *Geofizyczne odwzorowanie melanży w płytkich strefach pasm orogenicznych – przykład z pienińskiego pasa skałkowego*. Wydawnictwa AGH, Kraków, pp. 35–57. [In Polish.]

Golonka, J., Chowaniec, J. & Waśkowska, A., 2025. Outline of the geological structure of the western part of the Pieniny Klippen Belt. *Annales Socetatis Geologorum Poloniae*, 95: 1–16.

Golonka, J. & Krobicki, M., 2004. Jurassic paleogeography of the Pieniny and Outer Carpathian basins. *Rivista Italiana di Paleontologia e Stratigrafia*, 110: 5–14.

Golonka J., Krobicki M., Waśkowska, A., Cieszkowski, M. & Ślączka, A., 2017. Discussion of olistostromes of the Pieniny Klippen Belt, Northern Carpathians. *Geological Magazine*, 154: 193–200.

Golonka, J., Pietsch, K. & Marzec, P., 2018. The North European Platform suture zone in Poland. *Geology, Geophysics & Environment*, 44: 5–16.

Golonka, J., Pietsch, K., Marzec, P., Kasperska, M., Dec, J., Cichostępski, K. & Lasocki, S., 2019. Deep structure of the Pieniny Klippen Belt in Poland. *Swiss Journal of Geosciences*, 112: 475–506.

Golonka, J., Waśkowska, A., Cichostępski, K., Dec, J., Pietsch, K., Łój, M., Bania, G., Mościcki, W. J. & Porzucek, S., 2022. Mélange, flysch and cliffs in the Pieniny Klippen Belt (Poland): An overview. *Minerals*, 12: 1149.

Grabowska, T., Bojdys, G., Lemberger, M. & Medoń, Z., 2007. Geophysical-and-geological interpretation of gravity and magnetic anomalies in Polish Western Carpathians. *Geologia*, 33: 103–126.

Grelle, G. & Guadagno, F. M., 2009. Seismic refraction methodology for groundwater level determination: "Water seismic index". *Journal of Applied Geophysics*, 68: 301–320.

Gunn, P. J., 1975. Linear transformations of gravity and magnetic fields. *Geophysical Prospecting*, 23: 300–312.

Ismail, N. A., Saad, R., Nawawi, M., Nordiana, M. M., Ismail, N. H. & Mohamad, E. T., 2010. Identification of rippability and bedrock depth using seismic refraction. *AIP Conference Proceedings*, 1325: 137–139.

Łój, M., Porzucek, S. & Matwij, W., 2024. Grawimetryczne odwzorowanie melanży w płytkich strefach wybranego fragmentu pienińskiego pasa skałkowego. In: Golonka, J., Łój, M. & Waśkowska, A. (eds), *Geofizyczne odwzorowanie melanży w płytkich strefach pasm orogenicznych – przykład z pienińskiego pasa skałkowego*. Wydawnictwa AGH, Kraków, pp. 59–93. [In Polish.]

Loke, M. H., 2012. *Tutorial: 2-D and 3-D Electrical Imaging Surveys*. Geotomo Software, Malaysia, 76–94 pp.

Loke, M. H., Acworth, I. & Dahlin, T., 2003. A comparison of smooth and blocky inversion methods in 2D electrical imaging surveys. *Exploration Geophysics*, 34: 182–187.

Lu, D. B., Zhou, Q. Y., Junejo, S. A. & Xiao, A. L., 2015. A systematic study of topography effect of ERT based on 3-D modeling and inversion. *Pure and Applied Geophysics*, 172: 1531–1546.

Marzec, P., Golonka, J., Pietsch, K., Kasperska, M., Dec, J., Cichostępski, K. & Lasocki, S., 2020. Seismic imaging of mélanges – Pieniny Klippen Belt case study. *Journal of the Geological Society*, 177: 629–646.

Metwaly, M. & AlFouzan, F., 2013. Application of 2-D geoelectrical resistivity tomography for subsurface cavity detection in the eastern part of Saudi Arabia. *Geoscience Frontiers*, 4: 469–476.

Mikołajczak, M., Barmuta, J., Ponikowska, M., Mazur, S. & Starzec, K., 2021. Depth-to-basement study for the western Polish Outer Carpathians from three-dimensional joint inversion of gravity and magnetic data. *Journal of Geoscience*, 66: 15–36.

Moritz, H., 2000. Geodetic Reference System 1980. *Journal of Geodesy*, 74: 128–133.

NurAmalina, M. K. A., Nordiana, M. M., Bery, A. A., Anuar, M. N. A., Maslinda, U., Sulaiman, N., Saharudin, M. A., Hisham, H., Nordiana, A. N. & Taqiuddin, Z. M., 2017. Application of 2-D resistivity imaging and seismic refraction method in identifying the structural geological contact of sedimentary lithologies. *Earth and Environmental Science*, 62: 012005.

Olona, J., Pulgar, J. A., Fernández-Viejo, G., López-Fernández, C. & González-Cortina, J. M., 2010. Weathering variations in a granitic massif and related geotechnical properties through seismic and electrical resistivity methods. *Near Surface Geophysics*, 8: 585– 599.

Porzucek, S. & Loj, M., 2021. Microgravity survey to detect voids and loosening zones in the vicinity of the mine shaft. *Energies,* 14: 3021.

Porzucek, S., Loj, M. & Golonka, J., 2023. Lineaments in the gravity image of the border zone between the Central and Outer Carpathians. *Minerals*, 13, 995.

Sheehan, J. R., Doll, W. E. & Mandell, W. A., 2005. An evaluation of methods and available software for seismic refraction tomography analysis. *Journal of Environmental and Engineering Geophysics*, 10: 21–34.

Sjödahl, P., Dahlin, T. & Zhou, B., 2006. 2.5D resistivity modelling of embankment dams to assess influence from geometry and material properties. *Geophysics,* 71: G107–G114.

Stefaniuk, M., Klityński, W., Jarzyna, J. & Golonka, J., 2007. The structure of the Carpathian overthrust and its basement in the Polish Western Carpathians in the light of reinterpretation of selected regional magnetotelluric profiles. *Geologia*, 33: 143–166.

Swartz, C. A., 1954. Some geometrical properties of residual maps. *Geophysics*, 19: 46–70.

Telford, W. M., Geldart, L. P. & Sheriff, R. E., 1990a. *Applied Geophysics*, *2nd Ed*. Cambridge University Press, Cambridge, UK, pp. 11–15.

Telford, W. M., Geldart, L. P. & Sheriff, R. E., 1990b. *Applied Geophysics*, *2nd Ed*. Cambridge University Press, Cambridge, UK, pp. 158–162.

Waśkowska, A. & Golonka, J., 2024. Melanże na tle rozwoju geodynamicznego pienińskiego pasa skałkowego. In: Golonka, J., Łój, M. & Waśkowska, A. (eds), *Geofizyczne odwzorowanie melanży w płytkich strefach pasm orogenicznych – przykład z pienińskiego pasa skałkowego*. Wydawnictwa AGH, Kraków, pp. 13–34. [In Polish.]

Waśkowska, A. & Golonka, J., 2025. Mélanges against the background of the geodynamic development of the Pieniny Klippen Belt. *Annales Societatis Geologorum Poloniae*, 95: 29–43.

Woźniak, T. & Bania, G., 2019a. Analysis of the tectonic and sedimentary features of the southern margin of the Krzeszowice Graben in southern Poland based on an integrated geoelectrical and geological studies. *Journal of Applied Geophysics*, 165: 60–76.

Woźniak, T. & Bania, G., 2019b. Integrated geoelectrical and geological data sets for shallow structure characterization of the southern margin of the Krzeszowice Graben (southern Poland). *Data in Brief*, 25: 104157.

Woźniak, T., Bania, G., Mościcki, W. J. & Ćwiklik, M., 2018. Electrical resistivity tomography (ERT) and sedimentological analysis applied to investigation of Upper Jurassic limestones from the Krzeszowice Graben (Kraków Upland, southern Poland). *Geological Quarterly*, 62: 287–302.

Yilmaz, O., 2001. *Seismic Data Analysis*. Society Of Exploration Geophysicists, Tulsa, USA

Zainal, M., Munir, B., Abakar, M., Yanis, M. & Muhni, A., 2021. Characterization of landslide geometry using seismic refraction tomography in the GayoLues, Indonesia. *Journal of Physics and its Applications*, 3: 148–154.

Zhang, J. & Toksöz, M. N., 1998. Nonlinear refraction traveltime tomography. *Geophysics*, 63: 1726–1737.

www.geoportal.gov.pl/dane/numeryczny-model-terenu
www.geoportal.gov.pl/pl/dane/ortofotomapa-orto/